Elsevier Editorial System(tm) for
International Journal of Hydrogen Energy
Manuscript Draft

Manuscript Number: HE-D-19-00914R1

Title: Reversible operation performance of microtubular solid oxide cells with a nickelate-based oxygen electrode

Article Type: SI:WHEC2018 (de Miranda)

Section/Category: Fuel Cells & Applications

Keywords: SOFC; fuel cell; electrolysis; nickelate; microtubular

Corresponding Author: Dr. miguel A laguna-bercero,

Corresponding Author's Institution: ICMA (CSIC-Unizar)

First Author: Miguel A Morales-Zapata

Order of Authors: Miguel A Morales-Zapata; Angel Larrea; miguel A laguna-bercero

Abstract: This paper describes the reversible operation of a highly efficient microtubular solid oxide cell (SOC) with a nickelate-based oxygen electrode. The fuel cell was composed of a microtubular support of nickel and yttria stabilized zirconia (Ni-YSZ), an YSZ dense electrolyte, and a double oxygen electrode formed by a first composite layer of praseodymium nickelate (PNO) and gadolinium-doped ceria (CGO) and a second one of PNO. A good performance of the cell was obtained at temperatures up to 800°C for both fuel cell (SOFC) and electrolysis (SOEC) operation modes, specially promising in electrolysis mode. The current density in SOEC mode at 800°C is about -980mA*cm-2 at 1.2V with 50% steam. Current density versus voltage curves (j-V) present a linear behavior in the electrolysis mode, with a specific cell area resistance (ASR) of 0.32 Ω.cm-2. Durability experiments were carried out switching the voltage from 0.7V to 1.2V. No apparent degradation was observed in fuel cell mode and SOEC mode up to a period of about 100 hours. However, after this period especially in electrolysis mode there is an accumulated degradation associated to nickel coarsening, as confirmed by SEM and EIS experiments. Those results confirm that nickelate based oxygen electrodes are excellent candidates for reversible SOCs.

Reversible operation performance of microtubular solid oxide cells with a nickelate-based oxygen electrode

M. A. Morales-Zapata[1,2], A. Larrea[1] and M. A. Laguna-Bercero[1*]

[1]Instituto de Ciencia de Materiales de Aragón, c/ María de Luna 3, 50018 Zaragoza, Spain

[2]Universidad Tecnológica de Panamá, av/ Ricardo J. Alfaro, Campus Víctor Levi Sasso, 0819-07289, Panama

*Corresponding author: malaguna@unizar.es

Abstract

This paper describes the reversible operation of a highly efficient microtubular solid oxide cell (SOC) with a nickelate-based oxygen electrode. The fuel cell was composed of a microtubular support of nickel and yttria stabilized zirconia (Ni-YSZ), an YSZ dense electrolyte, and a double oxygen electrode formed by a first composite layer of praseodymium nickelate (PNO) and gadolinium-doped ceria (CGO) and a second one of PNO. A good performance of the cell was obtained at temperatures up to 800°C for both fuel cell (SOFC) and electrolysis (SOEC) operation modes, specially promising in electrolysis mode. The current density in SOEC mode at 800°C is about -980mA·cm^{-2} at 1.2V with 50% steam. Current density versus voltage curves (*j*-*V*) present a linear behavior in the electrolysis mode, with a specific cell area resistance (ASR) of 0.32 Ω.cm^{-2}. Durability experiments were carried out switching the voltage from 0.7V to 1.2V. No apparent degradation was observed in fuel cell mode and SOEC mode up to a period of about 100 hours. However, after this period especially in electrolysis mode there is an accumulated degradation associated to nickel coarsening, as confirmed by SEM and EIS experiments. Those results confirm that nickelate based oxygen electrodes are excellent candidates for reversible SOCs.

1. Introduction

Solid oxide cell (SOC) technology is one of the most efficient systems for transforming chemical energy into electrical energy [1]. This technology can work in reversible mode (RSOC), producing hydrogen from steam and electricity (in solid oxide electrolysis mode, SOEC), and then use the stored hydrogen to generate electricity and heat (in fuel cell mode, SOFC), acting as an electrical energy storage device. The operation of SOCs at intermediate to high temperatures has the potential to provide large-scale electricity storage at a lower cost than other storage methods such as batteries, which would allow further development of renewable electricity sources as that is the case of solar and wind energy. Even so, applications for electricity storage in reversible mode (RSOC) are still limited [2].

However, there is a problem of long-term stability of the cell components at temperatures higher than 800ºC [3]. We have to bear in mind that 40,000 hours of operation is usually required for stationary devices and 1,000-20,000 hours for portable and transport devices [4]. For this reason, SOCs are typically developed with electrode materials for operations at intermediate temperatures, in the range between 600-800 ºC [5,6]. The characterization of reversible cells has been published extensively, especially for planar configuration. However, long-term reversibility has only been studied more recently [7,8,9,10,11,12,13,14,15]. In terms of degradation, one important issue is related with the presence of impurities or secondary phases at the electrolyte/electrode, which affect particularly to yttria-stabilized zirconia (YSZ) and ceria gadolinium oxide (CGO) [16,17]. Those impurities are generally segregated at the grain boundaries decreasing the ionic conductivity of the electrolytes [18]. In addition, cation diffusion can be t also aking place during cell operation, especially through the cell interphases. For example, Sm and Y segregation, as well as nickel agglomeration, was found on microtubular cells operated for periods above 1000 hours, leading to structural and chemical changes on the different layers [19]. The interaction between the barrier layer and the YSZ, could also result in the formation of solid solutions with a lower ionic conductivity [20].

Another issue is related to impurities coming from the fuel gas, producing the degradation of Ni-YSZ fuel electrodes [21]. The optimization of Ni-YSZ structures has also been studied, focusing on the correlation between the initial Ni-YSZ microstructure and the resulting electrochemical performance during long-term SOEC operation at high current density and (~0.9 atm) [22]. The present study demonstrated the advantages of decreasing Ni particle size, matching the particle size of the 3 different phases involved: Ni, YSZ and pores. It is evident that porosity distribution of the supports plays a very important role in electrolysis mode [23]. In this sense, it was recently reported that the introduction of large straight open pores into the supporting electrode allows fast diffusion and thus the concentration polarization contribution to the final resistance is reduced, providing better access to the reaction sites [24]. Finally, another important aspect to take into account when operating in SOEC mode is the limiting operation voltage. As previously reported by several authors, high voltages can lead to electronic reduction of the YSZ [25,26]. This is a consequence of a moderate increase in relation to the oxygen partial pressure in the adjacent gas phase occurs along the oxygen electrode/electrolyte interface. Severe cell degradation can be produced in form of voids, cracks and/or delamination of the oxygen electrode [10,27,28].

In order to solve all this problems, one way to reduce the cell degradation is to alternate cathodic (SOFC) and anodic (SOEC) operation modes [18]. For instance, it is possible to unblock a degraded Triple Phase Boundary (TPB: where pores meet the electronic and ionic conducting phases) by in-situ forming a new one by reversing the operation mode. Activation by reorganizing the Ni-YSZ interfaces can be achieved by reoxidizing the Ni particles, either by exposure to air or by a high polarization in SOEC mode, followed by the reduction back to Ni, leading to a new TPB and improving the electrochemical activity [29,30]. It has been also proposed to use high periodic cathodic polarizations that lead to the formation of a nanostructured Ni-YSZ with greater activity in TBP [31,32]. In terms of oxygen electrode activation/deactivation processes, it has been shown that in LSM-YSZ electrodes reversible operation either avoids the formation of oxygen bubbles at the electrolyte/electrode interface or enables reversal growing process [33]. When SOEC polarization is halted, the oxygen pressure is

released, and the grain boundaries are healed by sintering back together at the high operation temperature. Performance recovery was also demonstrated using LSCF-based electrodes in SOFC mode [34]. In this case, the degradation was attributed to surface segregation of Sr and accumulation at the electrode/electrolyte interface by cathodic polarization, and could be remarkably mitigated by anodic polarization.

On the other hand, the development of new enhanced oxygen electrodes is necessary to improve the phase stability and performance of the electrode/electrolyte interface under high in SOEC operation mode, and especially above ~ 750°C [35]. In this sense, nickelates pertaining to the Ruddlesden-Popper (RP) series are proposed as good candidates. The RP structure can be described by alternating “n” octahedral layers with perovskite structure, $(AMX_3)_n$, with rock-salt layers, AX, where A is a lanthanide or alkaline earth metal, M a transition metal and X the anion (general formulation: $A_{n+1}M_nX_{3n+1}$). As for the nickelates where A= La, Nd or Pr, high order RP oxides ($A_3Ni_2O_7$ and $A_4Ni_3O_{10}$) show fast ionic and electronic transport properties [36,37]. This family of materials presents a flexible oxygen stoichiometry, capable of accommodating the oxygen excess under high atmospheres in the crystallographic interstices and supporting the low atmospheres through the loss of interstitial oxygen. Nickelates show rapid diffusion of oxygen ions through granules and rapid surface exchange kinetics. Their oxygen diffusion and kinetic surface exchange coefficients are among the highest values available in literature [38]. It has also been reported that nickelates are less prone to Cr poisoning from interconnectors than LSCF based oxygen electrodes [39]. However, chemical and thermodynamic stability is a problem for the $Pr_3Ni_2O_7$ phase (PNO), the one with the highest oxygen diffusion and surface exchange kinetics, at the typical SOC operation temperatures [40]. In despite of this, nickelate materials have been proposed as oxygen electrodes for electrolysis applications [41,42]. Studies about reversibility using PNO cathodes were also performed in standard planar cells [43]. In addition, in a recent study we reported good stability using PNO-CGO oxygen electrodes, where no degradation was detected during 100 hours of SOFC operation. The performance obtained during these experiments in SOEC mode was also remarkable (-780mA·cm^{-2} at 800 ºC and 1.3V) [14]. In this

experiment it was concluded that a reaction between PNO and CGO occurs during sintering, thus forming a mixed oxide of cerium doped with Gd and Pr.

The present work will be focused on the development of advanced SOCs using PNO electrodes in microtubular configuration. This configuration presents significant advances including higher energetic density, better resistance to thermal stresses, and smaller starting times as compared with conventional planar configuration [13,44]. Several studies can be found in the literature regarding microtubular SOECs [10, 14, 15, 23]. In addition, Chen et al. [45] conducted direct synthesis of methane from CO_2-H_2O co-electrolysis using tubular SOCs. However, there is still lack in the literature about long-term reversibility studies using microtubular configuration. In our previous work, we presented results about the performance of PNO based cells in fuel cell and electrolysis mode [14]. Nevertheless, reversible cycling studies were not performed in detail, as they will be here presented and discussed.

2. Materials and methods

The support tubes were fabricated by the Powder Extrusion Molding (PEM) method, as previously described [46,47]. After reduction of nickel oxide their composition was 25% Ni, 25% YSZ and 50% porosity (in vol.%). YSZ electrolyte and the PNO based oxygen electrode were subsequently deposited by dip-coating. The oxygen electrode is composed of an external layer of PNO (Marion Technologies), and a functional PNO-CGO layer with 4:1 wt% composition (CGO from Fuelcellmaterials). Both layers were sintered in two steps at 1100º C for 2 hours. The final dimensions of the cells are: 580 µm thick fuel electrode, 20 µm thick YSZ electrolyte, 5 µm thick PNO-CGO and 40 µm thick PNO oxygen electrode (3.2 mm resulting diameter). The porosity of the samples was calculated by Hg porosimetry experiments, as described in reference [46]. The cells were then evaluated in SOFC and SOEC modes, using a fuel composition of 50% H_2 and 50% H_2O, using typical gas flows of 100 ml min^{-1} (fuel utilization of about 40%) [48]. The oxygen electrode was exposed to static air. Electrical contacts were made using gold wires in a four-probe setup configuration [49]. For the fuel electrode contact, gold wires were coiled into featured holes on both ends of the microtubes. For the oxygen electrode contact, gold wires were coiled around the PNO cathode surface (1 cm^2) adding Au paste to improve the electrical contact and current collection. The cells

were sealed to alumina tubes using a ceramic sealant (Aremco, Ceramabond 503). Current density–voltage (*j*-*V*) characteristics were recorded using a galvanostat/potentiostat (Princeton Applied Research, Oak Ridge, US) working in potentiodynamic mode at a scan rate of 5 $mV \cdot cm^{-2} \cdot s^{-1}$. Electrochemical impedance spectroscopy (EIS) measurements were performed under open circuit voltage (OCV) conditions using 20 mV of sinusoidal amplitude and a frequency range from 100 kHz to 100 mHz. The durability tests were carried out in chronoamperometry mode at fixed voltages of 0.7 V (SOFC mode) and 1.2 V (SOEC mode). The microstructure of the cell was analyzed, before and after operation, using a Carl-Zeiss (Merlin) field emission scanning electron microscope (FE-SEM).

3. Results and Discussion

The j-V curve measured at 800 ºC for the reversible microtubular Ni-YSZ/YSZ/PNO-CGO/PNO cell is shown in Fig. 1. The obtained current densities are about 500 $mAcm^{-2}$ at 0.7V in SOFC mode, and about -800 $mAcm^{-2}$ at 1.2V in SOEC mode (ASR_{SOFC} = 0.40 Ωcm^2 and ASR_{SOEC} = 0.32 Ωcm^2), and the performance is enhanced after 20 hours under SOEC operation: 580 $mAcm^{-2}$ at 0.7V in SOFC mode, and about -980 $mAcm^{-2}$ at 1.2V in SOEC mode (see figure 3a). The performance in SOFC mode, including power densities, is shown in figure 3b. These results outperform previous reversible microtubular cells in SOEC mode using either LSM-YSZ (-480 $mAcm^{-2}$ at 1.2V and 820 ºC) or LSCF (-675 $mAcm^{-2}$ at 1.2V and 800 ºC) as oxygen electrodes [10,15,47,50]. In despite of a slightly lower performance in fuel cell mode, it is remarkable that the performance on SOEC mode is significantly higher when using PNO-based oxygen electrodes. As previously reported, electrode materials with oxygen hyperstoichiometry due to their Ruddlesden–Popper crystal structure, such as PNO, are believed to be suitable for effective oxygen evolution in the SOEC mode [7].

Subsequent to the initial characterization, durability experiments were carried out. For this purpose, alternate SOFC and SOEC cycles were recorded fixing the voltage at 0.7 and 1.2 V respectively, as shown in Fig. 2. Representative *j*-V curves obtained between the cycles are shown in Fig 3. The total duration of the test was about 150 hours under

current load. As observed in Fig 3, an enhancement in terms of performance was obtained for both SOFC and SOEC modes after the first SOEC cycle at 1.2 V. In fact, maximum values of 600 $mA \cdot cm^{-2}$ at 0.7V (SOFC mode) and about -980$mA \cdot cm^{-2}$ at 1.2V (SOEC mode) were then obtained. Continuing the alternate durability test, no degradation was observed after the first SOFC cycle, but then, a clear loose of performance was perceived during the second SOEC cycle. In despite of this degradation, switching again to SOFC mode (second SOFC cycle) seems to be beneficial, as the current density increases with time until reaching a quasi-stationary state. As shown in Fig. 2, the degradation observed in SOEC mode is then recovered after the second SOFC cycle, and no apparent degradation was observed up to a period of about 100 hours. This behavior also occurs in both the third and fourth cycles. It is then clear that the system recovers its performance to a large extent by reversing between SOEC/SOFC modes. According to Graves et al. [33], formation of O_2 bubbles are being produced during extended SOEC operation by high internal pressures at the oxygen/electrolyte electrode interface and thus generating pore formation. As a consequence, continuous operation under electrolysis mode can carry out the complete separation of the YSZ particles at the oxygen electrode/electrolyte interface. The reversible operation either mitigates this mechanism or reverses its formation. Nevertheless, in our experiments not all the degradation is fully recovered and some of the decay is irreversible. After this period especially in electrolysis mode there is an accumulated degradation associated to nickel coarsening, as later confirmed by SEM and EIS experiments. The current fluctuations that can be observed in figure 2 were associated with partial contact losses in inner current collector. The anode contact was rebuilt after 60 hours (t_3) and then current fluctuations disappeared up to 125 hours (t_6), where they appeared again. Finally, the j–V curve at t_6 in SOEC mode shows a concave shape. At low current densities, concentration polarization can be observed possible as a consequence of the deterioration of the Ni-YSZ microstructure. Subsequently, the slope decreases at high current densities caused by electroreduction of the YSZ in the presence of the low oxygen partial pressures at the hydrogen electrode side [5, 27].

EIS measurements (Fig. 4) were also recorded at the end of each cycle in order to study the evolution of the cell. The Nyquist plots were fitted using the following

equivalent circuit: , where is an inductance, is the ohmic resistance, and , are resistances (R_i) in parallel with constant phase elements (CPE_i). Capacitance and frequencies for of each contribution were calculated according to the equations listed in reference [51]. The assignation of the fitting parameters to the different physicochemical processes according to their characteristic frequencies is, in general, consistent with previous results found in the literature for similar cells [14,52,53,54,55]. A summary of the fitting parameters is listed in Table 1. In order to validate the fitting, Distribution of Relaxation Times (DRT) analysis [56,57,58] was also performed, as described in the supplementary material, and the obtained values are also included in Table 1. The ohmic resistance (R_s) increased slightly during the degradation test. We believe that this could be related to coarsening of the gold paste of the oxygen electrode current collector, since no porosity was detected inside the YSZ electrolyte, a common cause for this fact frequently found by other authors [59]. R1 parameter is influenced by interface impurities such as $Pr_2Zr_2O_7$. This is probably the effect occurring at grain boundaries during sintering, or even during operation under current load. As observed in Table 1, this component is about constant with time after the first cycle. R2 and R3 parameters were assigned to charge transfer processes at the fuel and oxygen electrode, respectively. Focusing on R2, the variation of this component is probably associated to Ni growth and/or the formation of nickel hydroxides [60]. R2 values decreased after the SOFC cycles, while in SOEC conditions the opposite occurred, indicating a direct relation with the increase of steam. These processes related to charge transfer activation of the Ni phase [48,61], are possibly influenced by the agglomeration/expansion of the nickel particles in the fuel electrode, caused by steam partial pressure variations. The migration of Ni from the electrode/electrolyte interfaces to more distant zones has been previously reported [62,63,64], and could explain the increase of R2 due to charge transfer processes at the Ni-YSZ interface. In fact, YSZ-NiO crystallographic orientation is of great relevance for the reduction of NiO and the stability of the Ni-YSZ interface [65,66]. Under high applied voltages (1.2V) in a prolonged manner, Ni can be subjected to partial reoxidations. In relation to R3, apparently there is less variation with time of this component, which is associated to

charge transfer at the oxygen electrode. These oscillation is more noticeable from the DRT analysis, and could be attributed to the metastability of the PNO phase in the range of 800–950 ºC under oxidizing atmospheres, as a reversible decomposition into $Pr_4Ni_3O_{10-x}$ and PrO_{2-y} was reported [67]. Finally, the evolution of R4, assigned to mass transfer processes, mainly in the supporting fuel electrode, is similar to that observed for R2. It is reasonable to accept that the mobility of nickel particles also changes pore distribution in the support, thus affecting gas diffusion processes. Additionally, for a better understanding of the different components, EIS varying the current density was performed for an analogue cell, and their results can be found in the supplementary material (figure S4 and table S2), confirming the assignation of the four resistance components.

Typical microstructure of the cell after operation is shown in Fig. 5. No apparent degradation in the double-layer oxygen electrode (PNO-CGO/PNO) is observed after the reversible durability test (figure 5b). On the contrary, visible degradation occurs mainly in the Ni-YSZ fuel electrode, where the agglomeration of nickel particles results in a gradient distribution of porosity, where an accumulation of pores is observed in the inner part of the tube. This effect is quite significant in the large pores originated from the pore former, as observed in Fig. 5c and in the magnified images (figs. 5d-g). This finding is probably causing the decrease of current density, which is also consistent with the EIS degradation results. We have demonstrated that the degradation could be partially removed by reversible cycling between the electrolysis and fuel cell modes, in agreement with previous results [20,26,27]. However, irreversible damage was not fully recovered. Additional experiments will be then needed to find the limits under continuous SOEC operation in order to avoid irreversible damage.

4. Conclusions

We have prepared reversible microtubular solid oxide cells for both SOFC and SOEC applications using Ni-YSZ cermet as support and fuel electrode, YSZ as electrolyte and PNO-based oxygen electrode. The stability of PNO as oxygen electrode has been here confirmed. We have determined high current densities in SOFC mode, 600 $mA \cdot cm^{-2}$ at

0.7 V and 800 ºC, and about -980 mA·cm^{-2} at 1.2 V and 800 ºC in SOEC mode, which is, to the best of our knowledge, the highest reported value for a microtubular electrolyzer. The cells were operated under continuous load for a total period of 150 hours combing SOEC and SOFC cycles. Although some degradation was observed during SOEC operation, part of this degradation was recovered when cycling to SOFC mode. The cause of the degradation was attributed to nickel mobility at the fuel electrode under high steam partial pressures. These experiments confirm that PNO/CGO mixtures are excellent candidates as oxygen electrode for SOFC/SOEC applications. However, further experiments are needed in order to totally avoid degradation in terms of power density.

Acknowledgments

This work was funded by the MAT2015-68078-R project, financed by the Spanish Government (Ministerio de Economía y Competitividad) and the Feder Program of the European Union. The use of Servicio General de Apoyo a la Investigacion-SAI, Universidad de Zaragoza is finally acknowledged for the use of the electron microscopy facilities.

References

1 S. C. Singhal and K. Kendall, "High Temperature Solid Oxide Fuel Cells: Fundamentals, Design and Applications." Elsevier, (2003).

2 Krog Ekman C, Jensen SH. Prospects for large scale electricity storage in Denmark. Energy Conv Management 2010; 51(6):1140-47.

3 Hauch A, Ebbesen SD, Jensen SH, Mogensen M. Solid Oxide Electrolysis Cells: Microstructure and Degradation of the Ni/Yttria-Stabilized Zirconia Electrode. J Electrochem Soc 2008; 155: B1184.

4 Yokokawa H, Tu H, Iwanschitz B, Mai A. Fundamental mechanisms limiting solid oxide fuel cell durability. J Power Sources 2008; 182:400-12.

5 Laguna-Bercero MA, Campana R, Larrea A, Kilner JA, Orera VM. Steam Electrolysis Using a Microtubular Solid Oxide Fuel Cell. J Electrochem Soc 2010; 157(6): B852-55.

6 Laguna-Bercero MA, Férriz A, Larrea A, Correas L, Orera VM. Long-Term Stability Studies of Anode-Supported Microtubular Solid Oxide Fuel Cells. Fuel Cells 2013; 13(6):1116–22.

7 Laguna-Bercero MA. Recent advances in high temperature electrolysis using solid oxide fuel cells: A review. J Power Sources 2012; 203: 4– 16.

8 Cable TL, Setlock JA, Farmer SC, Eckel AJ. Regenerative Performance of the NASA Symmetrical Solid Oxide Fuel Cell Design. Intl J App Ceram Tech 2011; 8(1):1-12.
9 Hughes G, Yakal-Kremski K, Barnett SA. Life Testing of LSM-YSZ composite electrodes under reversing-current operation. Phys Chem Phys 2013; 15(40):17257-62.
10 Laguna-Bercero MA, Campana R, Larrea A, Kilner JA, Orera VM. Performance and Aging of Microtubular YSZ-based Solid Oxide Regenerative Fuel Cells. Fuel Cells 2010 ; 11(1) :116–23.
11 Mougin J, Chatroux A, Couturier K, Petitjean M, Reytier M, Gousseau G, Lefebvre-Joud F. High Temperature Steam Electrolysis Stack with Enhanced Performance and Durability. Energy Procedia 2012; 29:445-54.
12 Graves C. Reversing and Repairing Microstructure Degradation in Solid Oxide Cells during Operation. ECS Transactions 2013; 57(1): 3127-36.
13 Orera VM, Laguna-Bercero MA, Larrea A. Fabrication methods and performance in fuel cell and steam electrolysis operation modes of small tubular solid oxide fuel cells: a review. Frontiers in Energy Research 2014;2.https://www.frontiersin.org/article/10.3389/fenrg.2014.00022. doi: 10.3389/fenrg.2014.00022.
14 Laguna-Bercero MA, Monzón H, Larrea A, Orera VM. Improved stability of reversible solid oxide cells with a nickelate-based oxygen electrode. J Mater Chem A 2016; 4:1446-53.
15 López-Robledo MJ, Laguna-Bercero MA, Larrea A, Orera VM. Reversible operation of microtubular solid oxide cells using La0.6Sr0.4Co0.2Fe0.8O3-δ-Ce0.9Gd0.1O2-δ oxygen electrodes. J Power Sources 2018; 378:184–89.
16 Baumann FS, Fleig J, Konuma M, Starke U, Habermeier HU, Maier J. Strong Performance Improvement of La0.6Sr0.4Co0.8Fe0.2O3-d SOFC Cathodes by Electrochemical Activation. J Electrochem Soc 2005; 152(10): A2074-79.
17 Tomkiewicz AC, Tamimi MA, Huq A, McIntosh S. FD electrolysis: is the surface oxygen exchange rate linked to bulk ion diffusivity in mixed conducting Ruddlesden–Popper phases?. Faraday Discuss 2015; 182: 113-27.
18 Hansen KV, Norrman K, Mogensen M. TOF SIMS studies of yttria stabilised zirconia. Surf Interface Anal. 2006; 38: 911 – 16.
19 Slodczyk A, Torrell M, Hornés A, Morata A, Kendall K, Tarancón A, Understanding longitudinal degradation mechanisms of large-area micro-tubular solid oxide fuel cells, Electrochimica Acta 2018; 265:232-243.
20 Morales M, Miguel-Pérez V, Tarancón A, Slodczyk A, Torrell M, Ballesteros B, Ouweltjes JP, Bassat JM, Montinaro D, Morata A, Multi-scale analysis of the diffusion barrier layer of gadolinia-doped ceria in a solid oxide fuel cell operated in a stack for 3000 h, J Power Sources 2016; 344:141-151.
21 Irvine JTS, Neagu D, Verbraeken MC, Chatzichristodoulou C, Graves C, Mogensen MB. Evolution of the electrochemical interface in high-temperature fuel cells and electrolysers. Nature Energy 2016;1:15014.
22 Hauch A, Brodersen K, Chen M, Mogensen MB. Ni/YSZ electrodes structures optimized for increased electrolysis performance and durability. Solid State Ionics 2016; 293:27–36.

23 Laguna-Bercero MA, Hanifi AR, Menand L, Sandhu NK, Anderson NE, Etsell TH, Sarkar P. The effect of pore-former morphology on the electrochemical performance of solid oxide fuel cells under combined fuel cell and electrolysis modes. Electrochimica Acta 2018; 268: 195-201.
24 Lin J, Chen L, Liu T, Xia C, Chen C, Zhan Z. The beneficial effects of straight open large pores in the support on steam electrolysis performance of electrode-supported solid oxide electrolysis cell. J Power Sources 2018; 374: 175-80.
25 Virkar A.V., Mechanism of oxygen electrode delamination in solid oxide electrolyzer cells. Int. J. Hydrogen Energy 2010; 35, 9527-43.
26 Lim HT, Virkar AV. Measurement of oxygen chemical potential in thin electrolyte film, anode-supported solid oxide fuel cells, J. Power Sourc. 2008; 180: 92-102.
27 Schefold J., Brisse A., Zahid, M. Electronic Conduction of Yttria-Stabilized Zirconia Electrolyte in Solid Oxide Cells Operated in High Temperature Water Electrolysis. J. Electrochem. Soc. 2009; 156, B897-04.
28 Mawdsley J. R., Carter J. D., Kropf A. J., Yildiz B. , Maroni V.A., Post-test evaluation of oxygen electrodes from solid oxideelectrolysis stacks. Int. J. Hydrogen Energy 2009; 34, 4198-07.
29 Knibbe R, Traulsen ML, Hauch A, Ebbesen SD, Mogensen M. Solid Oxide Electrolysis Cells: Degradation at High Current Densities. J Electrochem Soc 2010; 157 (8):B1209-17.
30 Chen K, Jiang SP. Failure mechanism of (La,Sr)MnO3 oxygen electrodes of solid oxide electrolysis cells. Int J Hydrog Energy 2011; 36:10541–49.
31 Tietz F, Sebold D, Brisse A, Schefold J. Degradation phenomena in a solid oxide electrolysis cell after 9000 h of operation. J Power Sources 2013; 223: 129–35.
32 Hughes GA, Railsback JG, Yakal-Kremski KJ, Butts DM, Barnett SA. Degradation of (La0.8Sr0.2)0.98MnO3-d–Zr0.84Y0.16 O2- composite electrodes during reversing current operation. Faraday Discuss 2015; 182:365-77.
33 Graves C, Ebbesen SD, Jensen SH, Simonsen SB, Mogensen MB. Eliminating degradation in solid oxide electrochemical cells by reversible operation. Nature Materials 2015; 14:239-44.
34 Hea Z, Zhang L, Hed S, Ai N, Chen K, Shao Y, Jiang SP. Cyclic polarization enhances the operating stability of La0.57Sr0.38Co0.18Fe0.72Nb0.1O3-d oxygen electrode of reversible solid oxide cells. J Power Sourc 2018; 404:73–80.
35 Momma A, Kato T, Kaga Y, Nagata S. Polarization Behavior of High Temperature Solid Oxide Electrolysis Cells (SOEC). J Ceram Soc Japan 1997; 105(5):369-73.
36 Amow G, Davidson IJ, Skinner SJ. A comparative study of the Ruddlesden-Popper series, Lan+1NinO3n+1 (n=1,2 and 3), for solid-oxide fuel cell cathode applications. Solid State Ionics 2006; 177(13-14):1205-10.
37 Zhang Z, Greenblatt M. Synthesis, Structure, and Properties of Ln4Ni3O10-δ (Ln = La, Pr, and Nd). J Solid-State Chem 1995;117(2):236-46.
38 Skinner SJ, Kilner JA. Oxygen diffusion and surface exchange in La2−xSrxNiO4+δ. Solid State Ionics 2000; 135(1-4):709–12.
39 Odier P, Allançon C, Bassat JM. Oxygen Exchange in Pr2NiO4+δ at High Temperature and Direct Formation of Pr4Ni3O10−x. J Solid State Chem 2010; 153 (2): 381-85.

40 Montenegro-Hernandez A, Vega-Castillo J, Mogni L, Caneiro A. Thermal stability of Ln2NiO4+δ (Ln: La, Pr, Nd) and their chemical compatibility with YSZ and CGO solid electrolytes. Intl J Hydrog Energy 2011;36(24):15704–14.
41 Egger A, Schrödl N, Gspan C, Sitte W. La2NiO4 + δ as electrode material for solid oxide fuel cells and electrolyzer cells. Solid State Ionics 2017; 299:18-25.
42 Chauveau F, Mougin J, Bassat JM, Mauvy F, Grenier JC. A new anode material for solid oxide electrolyser: The neodymium nickelate Nd2NiO4+δ. J Power Sources 2010; 195:744-49.
43 Vibhu V. Stability and ageing studies of praseodymium-based nickelates as cathodes for Solid Oxide Fuel Cells. Material chemistry. Universite de Bordeaux 2016. https://tel.archives-ouvertes.fr/tel-01424845/document. Last accesed on: 18 jan 2019.
44 Torrell M, Morata A, Kendall M, Kendall K, Tarancon A. Towards a high fuel utilization and low degradation of micro-tubular solid oxide fuel cells. Int J Hydrogen Energy 2017; 42; 13889-01.
45 Chen L, Chen F, Xia C, Direct synthesis of methane from CO2-H2O co-electrolysis in tubular solid oxide electrolysis cells, Energy Environ Sci 2014; 7: 4018-22.
46 Arias-Serrano BI, Sotomayor ME, Várez A, Levenfeld B, Monzón H, Laguna-Bercero MA, Larrea A. High-performance Ni–YSZ thin-walled microtubes for anode-supported solid oxide fuel cells obtained by powder extrusion moulding. RSC Advances 2016; 6: 19007-15.
47 Monzón H, Laguna-Bercero M.A, Larrea A, Arias BI, Várez A, Levenfeld B. Design of industrially scalable microtubular solid oxide fuel cells based on an extruded support. Int J Hydr Energy 2014; 39:5470–76.
48 Monzón H, Laguna-Bercero MA. Highly Stable Microtubular Cells for Portable Solid Oxide Fuel Cell Applications. Electrochim. Acta 2016; 222:1622-27.
49 Monzón H, Laguna-Bercero MA. Redox-cycling studies of anode-supported microtubular solid oxide fuel cells. Intl J Hyd Energy 2012; 37:7262-70.
50 Lopez-Robledo MJ, Laguna-Bercero MA, Silva J, Orera VM, Larrea A. Electrochemical performance of intermediate temperature micro-tubular solid oxide fuel cells using porous ceria barrier layers. Ceramics International 2015; 41: 7651-60.
51 Rieu M, Sayers R, Laguna-Bercero MA, Skinner SJ, Lenormand P, Ansarta F. Investigation of Graded La2NiO4+d Cathodes to Improve SOFC Electrochemical Performance. J Electrochem Soc 2010;157 (4): B477-80.
52 Chrzan A, Ovtar S, Jasinski P, Chen M, Hauch A. High performance LaNi1-xCoxO3-δ (x = 0.4 to 0.7) infiltrated oxygen electrodes for reversible solid oxide cells. J Power Sources 2017; 353:67-76.
53 Chen T, Liu M, Yuan C, Zhou Y, Ye X, Zhan Z, Xia C, Wang S. High performance of intermediate temperature solid oxide electrolysis cells using Nd2NiO4+δ impregnated scandia stabilized zirconia oxygen electrode. J Power Sources 2015; 276: 1-6.
54 Laguna Bercero MA, Luebbe H, Silva J, van Herle J. Electrochemical performance of Nd1. 95NiO4+ δ cathode supported microtubular solid oxide fuel cells. Fuel Cells 2015; 15:98-104.

55 Ogier IT, Mauvy F, Bassat JM, Laurencin J, Mougin J, Grenier JC. Overstoichiometric oxides Ln2NiO4+δ (Ln = La, Pr or Nd) as oxygen anodic electrodes for solid oxide electrolysis application. Intl J Hyd Energy 2015; 40(46):15885-92.
56 Saccoccio M, Wan TH, Chen C, Ciucci F. Optimal Regularization in Distribution of Relaxation Times applied to Electrochemical Impedance Spectroscopy: Ridge and Lasso Regression Methods – A Theoretical and Experimental Study. Electrochimica Acta 2014; 147:470-82.
57 Ciucci F, Chen C. Analysis of Electrochemical Impedance Spectroscopy Data Using the Distribution of Relaxation Times: A Bayesian and Hierarchical Approach. Electrochimica Acta 2015; 167:439-54.
58 Wan TH, Saccoccio M, Chen C, Ciucci F. Influence of the Discretization Methods on the Distribution of Relaxation Times Deconvolution: Implementing Radial Basis Functions with DRTtools. Electrochimica Acta 2015; 184:483-99.
59 The D, Grieshammer S, Schroeder M, Martin M, Al Daroukh M, Tietz F, Schefold J, Brisse A. Microstructural comparison of solid oxide electrolyser cells operated for 6100 h and 9000 h. J Power Sources 2015; 275:901-11.
60 Torrell M, Morata A, Kayser P, Kendall M, Kendall K, Tarancon A. Performance and long term degradation of 7 W micro-tubular solid oxide fuel cells for portable applications. J Power Sourc 2015; 285: 439-48.
61 Laguna-Bercero MA, Hanifi AR, Monzón H, Cunningham J, Etsell TH, Sarkar P. High Performance of Microtubular Solid Oxide Fuel Cells Using Nd2NiO4+a Based Composite Cathodes. J Mater Chem A 2014; 2:9764.
62 Pihlatie MH, Kaiser A, Mogensen MB, Chen M. Electrical conductivity of Ni-YSZ composites: Degradation due to Ni particle growth. Solid State Ionics 2011; 189 (1): 82-90.
63 Monzón H, Laguna-Bercero M. A. Highly Stable Microtubular Cells for Portable Solid Oxide Fuel Cell Applications. Electrochim. Acta 2016; 221:41-47.
64 Holzer L, Iwanschitz B, Hocker T, Münch B, Prestat M, Wiedenmann D, Vogt U, Holtappels P, Sfeir J, Mai A, Graule T. Microstructure degradation of cermet anodes for solid oxide fuel cells: Quantification of nickel grain growth in dry and in humid atmospheres. J Power Sourc 2011;196 (3):1279-94.
65 Jeangros Q, Faes A, Wagner JB, Hansen TW, Aschauer U, Van Herle J, Hessler-Wyser A, Dunin-Borkowski RE. In situ redox cycle of a nickel–YSZ fuel cell anode in an environmental transmission electron microscope. Acta Materialia 2010;58(14): 4578-89.
66 Laguna-Bercero MA, Larrea A. YSZ Induced Crystallographic Reorientation of Ni Particles in Ni–YSZ Cermets. J American Ceramic Society 2007; 90 (9): 2954-60.
67 Kovalevsky AV, Kharton VV, Yaremchenko AA, Pivak YV, Tsipis EV, Yakovlev SO, Markov AA, Naumovich EN, Frade JR. Oxygen permeability, stability and electrochemical behavior of Pr2NiO4+d based materials. J. Electroceram., 2007, 18, 205-218.

Figure

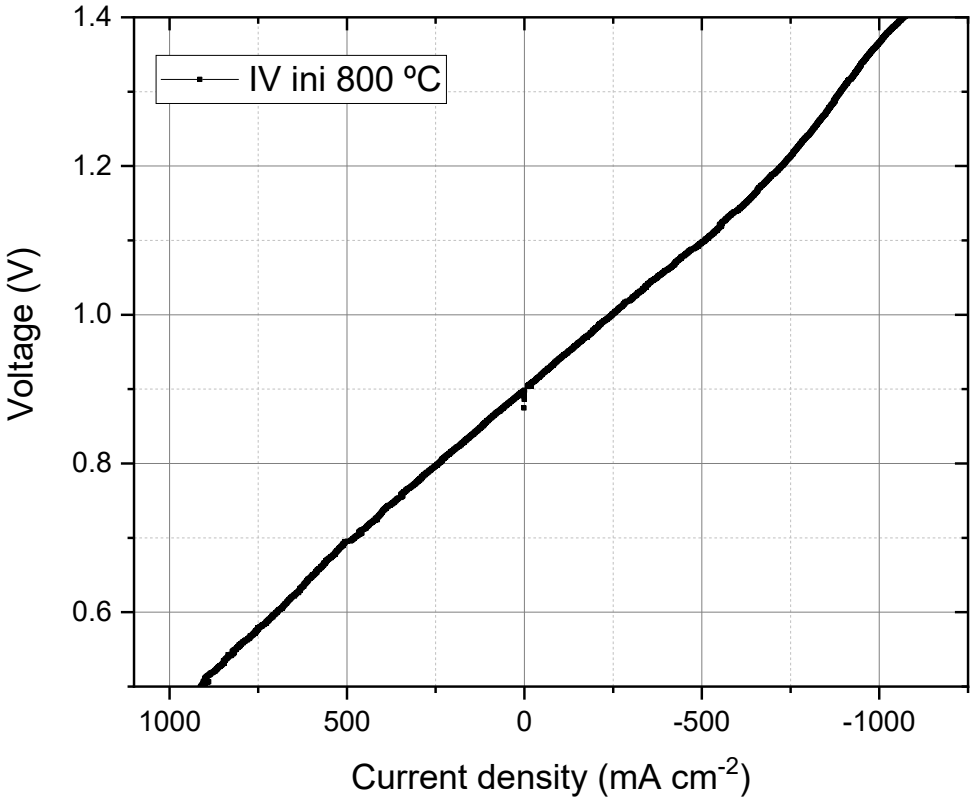

Figure 1. Initial *j*-V characterization (t_0) of the microtubular cell in SOFC/SOEC modes at 800ºC.

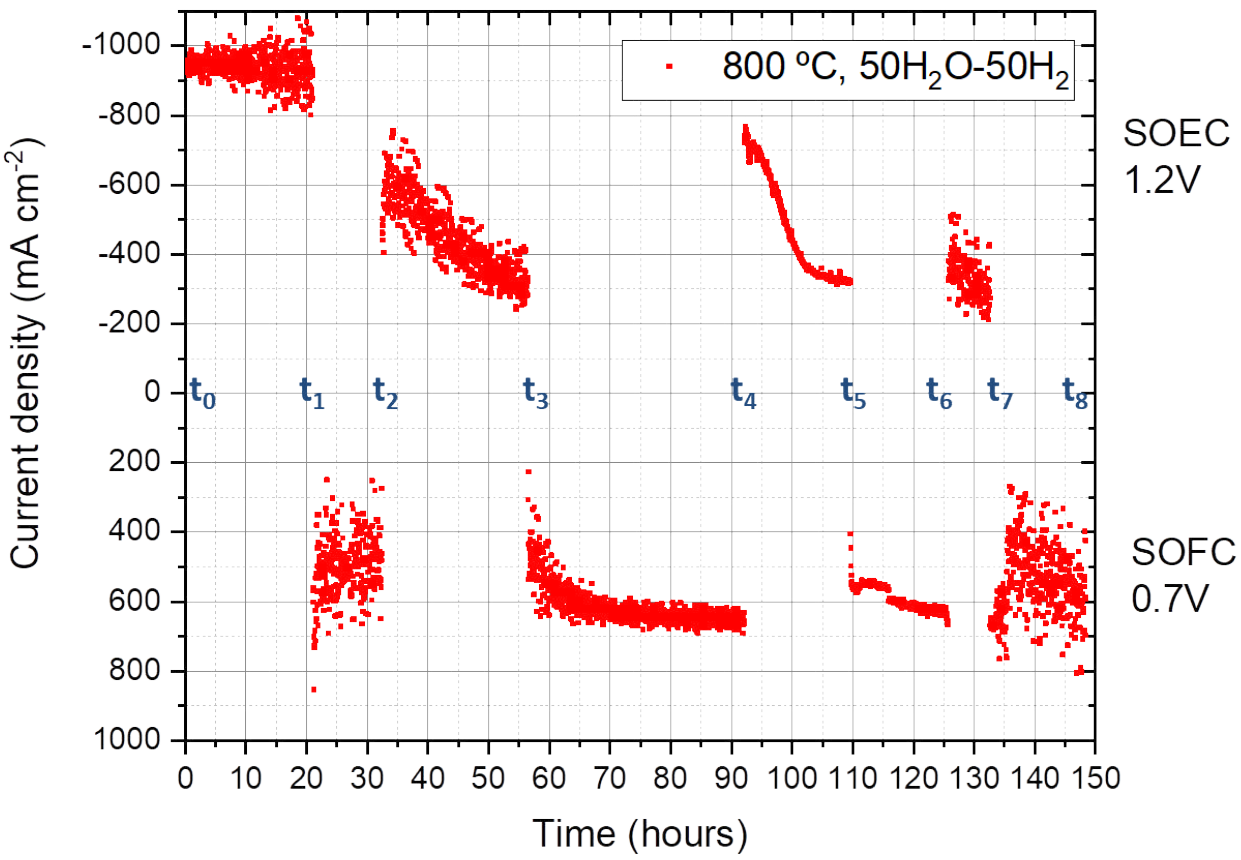

Figure 2. Durability tests in SOEC (1.2 V) and SOFC (0.7 V) modes. The different time intervals are shown in the graph (t_0-t_8).

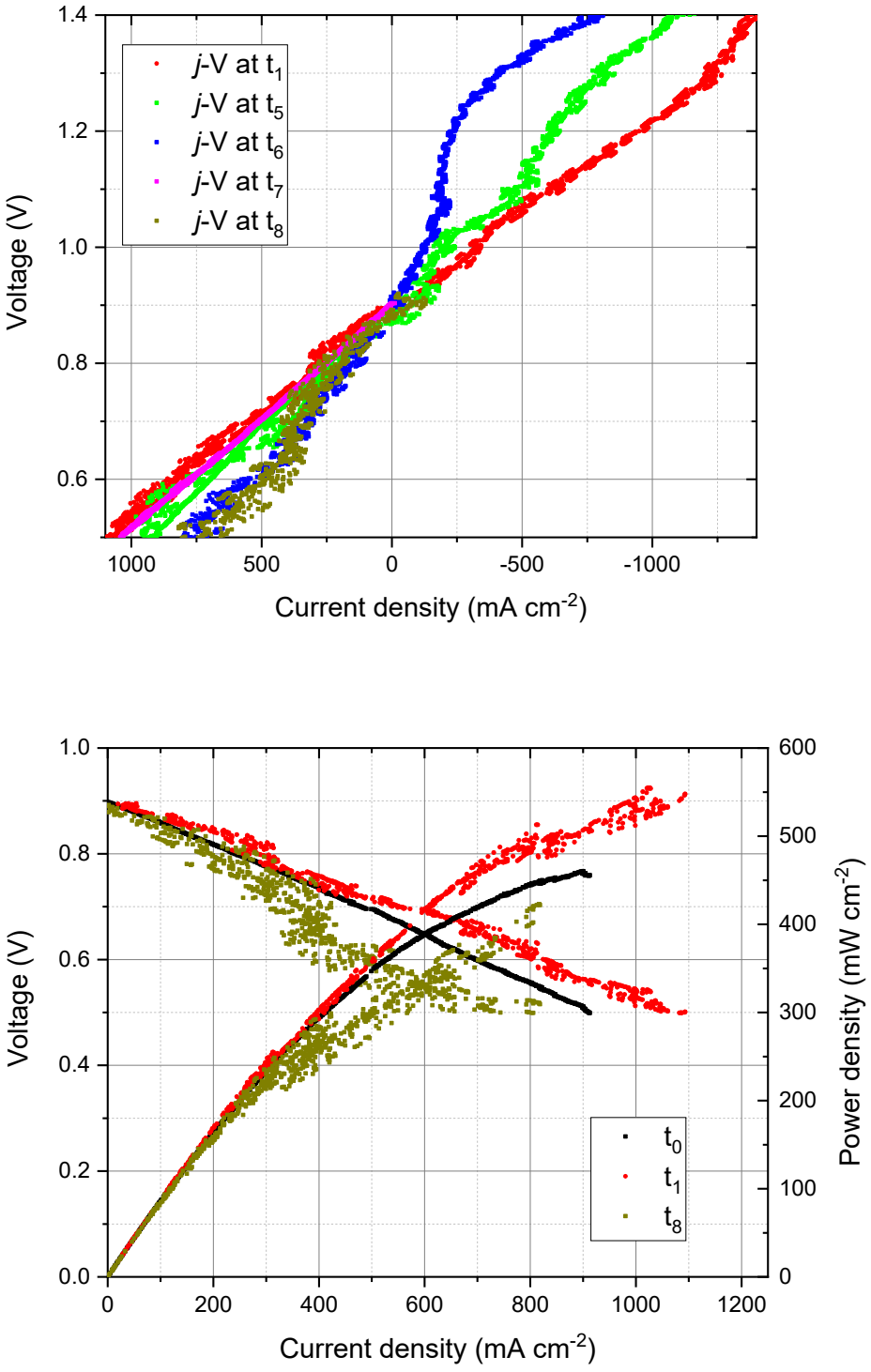

Figure 3. (a) *j*-V curves of the microtubular cell in SOFC/SOEC modes at 800ºC collected at different time intervals during the durability test; (b) *j*-P curves in SOFC mode at the initial state (t_0), after stabilization (t_1) and after the complete durability test (t_8).

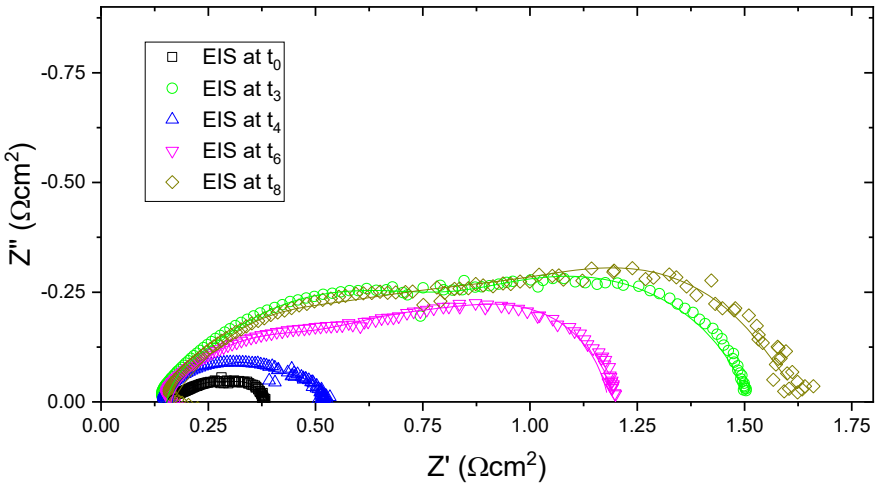

Figure 4. Nyquist plots at 800ºC (OCV conditions) collected at different time intervals during the durability test.

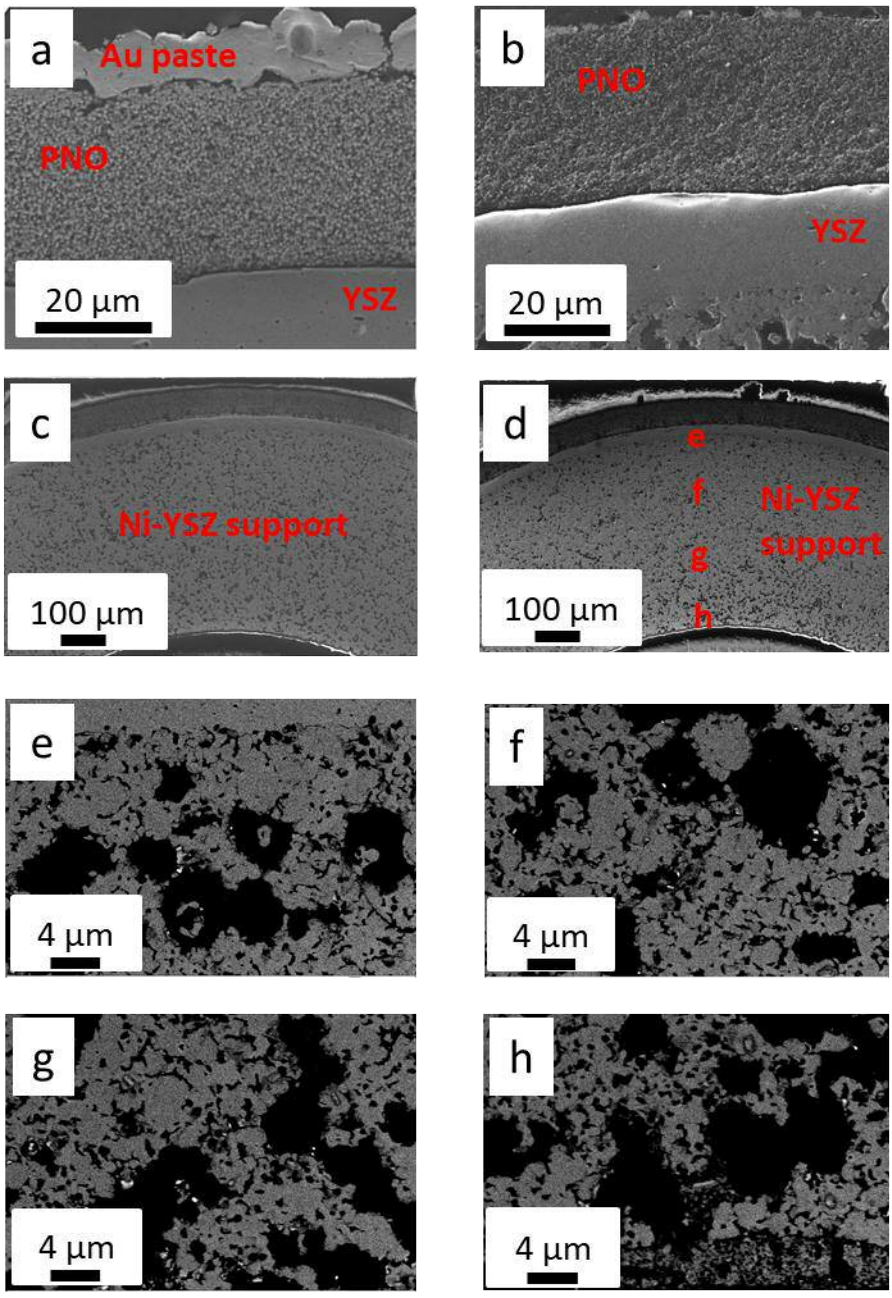

Figure 5. SEM images showing the microstructure microtubular cells before and after durability studies: a) Detail of the PNO electrode of an identical cell before operation; b) detail of the PNO electrode after operation; c) microstructure of a similar cell before operation showing an homogeneous distribution of porosity in the Ni-YSZ support; d) microstructure of the PNO cell after operation showing the evolution of the porosity in the Ni-YSZ support. Letters e-h indicate the approximate region where the subsequent images (magnified) where taken.

Table 1. Fitting values of the Nyquist plots collected at 800º C and OCV using equivalent circuits. Contributions to ASR correspond to the sum of R_s and R_{pol} (in $\Omega.cm^2$), with R_{pol}=R1+R2+R3+R4. Typical frequency range and capacity values for each contribution are also indicated. The values in parenthesis correspond with the calculated DRT values (see supplementary material).

Sample	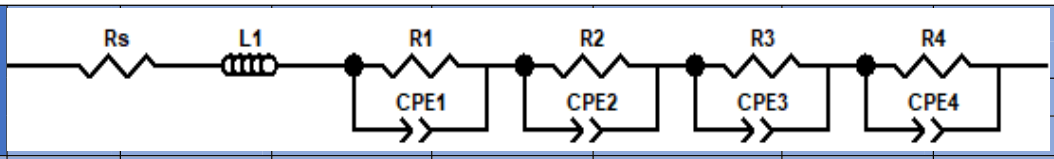						
Time collected	**R_s**	**R1 (2-15x10^3 Hz) (10^{-4} F cm-2)**	**R2 (400-1500 Hz) (~10^{-3} F.cm^{-2})**	**R3 (50-100 Hz) (~10^{-2} F.cm^{-2})**	**R4 (<12 Hz) (~10^{-1} F.cm^{-2})**	**R_{pol}**	**ASR_{cell}**
t_0 initial state	0.15 (0.15)	0.03 (0.04)	0.01 (0.06)	0.14 (0.07)	0.05 (0.07)	0.23 (0.23)	0.38 (0.38)
t_3 (56 h). after SOEC	0.16 (0.15)	0.09 (0.07)	0.24 (0.37)	0.29 (0.45)	0.73 (0.46)	1.35 (1.34)	1.51 (1.49)
t_4 (90 h). after SOFC	0.17 (0.16)	0.09 (0.04)	0.10 (0.12)	0.09 (0.06)	0.07 (0.07)	0.35 (0.29)	0.51 (0.45)
t_6 (125 h). after SOFC	0.18 (0.16)	0.11 (0.06)	0.19 (0.24)	0.17 (0.37)	0.56 (0.37)	1.02 (1.03)	1.20 (1.19)
t_8 (150 h). after SOFC	0.18 (0.17)	0.12 (0.09)	0.25 (0.36)	0.26 (0.49)	0.81 (0.48)	1.43 (1.43)	1.61 (1.60)

Supplementary Material

Click here to download Supplementary Material: Support document IJHE Morales.docx